

Design and characterization of a high-power ultrasound driver with ultralow-output impedance

George K. Lewis, Jr.¹ and William L. Olbricht^{1,2}

¹Department of Biomedical Engineering, Cornell University, Ithaca, New York 14853, USA

²School of Chemical and Biomolecular Engineering, Cornell University, Ithaca, New York 14853, USA

(Received 2 September 2009; accepted 13 October 2009; published online 10 November 2009)

We describe a pocket-sized ultrasound driver with an ultralow-output impedance amplifier circuit (less than 0.05Ω) that can transfer more than 99% of the voltage from a power supply to the ultrasound transducer with minimal reflections. The device produces high-power acoustical energy waves while operating at lower voltages than conventional ultrasound driving systems because energy losses owing to mismatched impedance are minimized. The peak performance of the driver is measured experimentally with a PZT-4, 1.54 MHz, piezoelectric ceramic, and modeled using an adjusted Mason model over a range of transducer resonant frequencies. The ultrasound driver can deliver a $100 V_{pp}$ (peak to peak) square-wave signal across 0–8 MHz ultrasound transducers in 5 ms bursts through continuous wave operation, producing acoustic powers exceeding 130 W. Effects of frequency, output impedance of the driver, and input impedance of the transducer on the maximum acoustic output power of piezoelectric transducers are examined. The small size, high power, and efficiency of the ultrasound driver make this technology useful for research, medical, and industrial ultrasonic applications. © 2009 American Institute of Physics.
[doi:10.1063/1.3258207]

I. INTRODUCTION

We present a new amplifier design and printed circuit board (PCB) schematic for an efficient ultrasound driver that can be incorporated easily into acoustic applications in science and engineering. The principle underlying the driver design is based on earlier work that used a low output impedance driver in a portable high intensity focused ultrasound (HIFU) system.¹ Here, we analyze an ultralow-output impedance driver that delivers high-current bursts, continuous wave, and frequency sweep operation for single element, phased-array, and time-reversal acoustic applications.

Ultrasound has had decades of great success as a diagnostic imaging modality, but in recent years studies have shown that the application of ultrasound can be an effective therapy or enhance existing therapies in a variety of clinical applications.^{2–5} For example, ultrasound has been used to lyse blood clots and to improve the action of thrombolytic agents.⁵ It has been used to temporarily break down the blood-brain barrier, to enhance the delivery of antitumor agents and other drugs, to occlude blood vessels, to cauterize wounds, and to enhance wound healing.^{5–9} Furthermore, HIFU potentially offers a new way to perform ablative surgery on a variety of organs including heart, liver, prostate, and brain.^{10–12} The acoustic power that is required varies among applications. Some applications require relatively low power levels for acoustic streaming and agitation effects.^{2,4} Other applications require high power levels, and in these cases tissue heating and acoustic cavitation are dominant effects.^{5,13–15}

Despite the potential of ultrasound-based therapies, their translation, and clinical implementation has been limited in part by the lack of cost-effective and convenient ways of

generating ultrasound over a wide range of power levels.¹ The basic method of producing ultrasound power has not changed significantly in 50 years.^{11,16,17} Most ultrasound driving systems are based on high-voltage switching devices or rf amplifiers that are customarily built with a 50Ω output impedance. The 50Ω output impedance is a historical standard based on the development in the 1930s of coax cables for kilowatt radio transmitters.¹⁸ The 50Ω impedance was chosen as a compromise between power handling and low loss in air-dielectric coax transmission cable. The 50Ω output impedance was subsequently used in laboratory electronic devices, and it is now an accepted standard for function generators, oscilloscopes, rf amplifiers, pulse generators, and other electronic instruments.

A consequence of this standard is that the output impedance of conventional ultrasound drivers does not match the characteristic electrical impedance of typical ultrasound transducers. The maximum power-transfer theorem states: *to obtain maximum external power from a source with finite internal impedance, the impedance of the load must be made the same as that of the source.* Therefore, the output impedance of the ultrasound driver is matched to that of the transducer using special impedance matching circuitry and automatic tuning devices.^{11,16,17} Even then, only 50% of the amplifier's voltage is delivered across the transducer with the other 50% dissipated as heat.

Taking a different approach, we have developed a low-voltage, high-power 0–8 MHz ultrasound driver with an ultralow-output impedance amplifier circuit (less than 0.05Ω) that can transfer more than 99% of the voltage from the power supply to the transducer. It produces acoustical energy waves at lower voltages than those in conventional

ultrasound drivers, since energy losses owing to mismatched impedance are eliminated. Since impedance matching circuitry is not required, the driver and PCB can be built for about \$100. Acoustic energy production from the driver was measured experimentally and modeled mathematically using an adjusted Mason model over a range of transducer frequencies.^{19,20} The performance of the driver with transducers connected directly to the driver's output was compared with its performance when traditional impedance matching was used. Results show that the ultrasound driver can deliver 100 V_{pp} square-wave signal across 0–8 MHz ultrasound transducers with pulsed current draws in excess of 10 A. Modeling and experimental measurements show that maximum acoustic output power depends on the impedance of the ultrasound transducer and the output impedance of the ultrasound driver.

II. METHODS

This section describes the ultrasound driver circuit, PCB design, and construction, modeling and measurements of acoustic energy production, and an evaluation of driver performance with and without impedance matching to the transducer. Component specifications and part numbers are listed in the appendix.

A. Circuit schematic

The design of the ultralow-impedance, high-current, transistor-transistor logic (TTL) ultrasound driver builds on principles that were demonstrated in a simple prototype.¹ The prototype used eight metal oxide semiconductor field effect transistors (MOSFETs) in parallel to deliver 50 W continuously without excessive heating of the MOSFETs. The present design uses additional MOSFETs to reduce the current through each MOSFET and to reduce the output impedance of the driver, which increases output power, provided there are no limitations from the power source.

Figure 1 is a schematic of the driver, which uses 14 MOSFETs in parallel to generate the driver output. A branched tree of pin drivers provides signals to the MOSFETs so that they switch synchronously. Each pin driver and MOSFET in Fig. 1 is analogous to the pin driver and MOSFET used in the prototype, except that a single pin driver switches multiple MOSFETs in the present arrangement.

The first pin driver (EL71881SZ), shown at the left in Fig. 1, is capable of driving high capacitive loads. A 5–10 V square wave from a crystal oscillator or function generator is supplied to pin 3 of the pin driver. Pins 1 and 8 are held at +5 V with 10 and 0.1 μF bypass capacitors to ground (not shown in Fig. 1). Pin 2 is connected to pin 1 with a 10 k Ω resistor. Pins 4–6 are connected to earth ground. The output from pin 7 provides a 5 V square wave to drive the second generation of pin drivers. These pin drivers provide a 5 V square wave to the third generation of pin drivers, which regulate switching of the MOSFET's voltage drain. These four pin drivers are held at +12 V instead of +5 V because +12 V is the optimal voltage for MOSFET switching. The outputs of these pin drivers are split with two 0.1 μF cou-

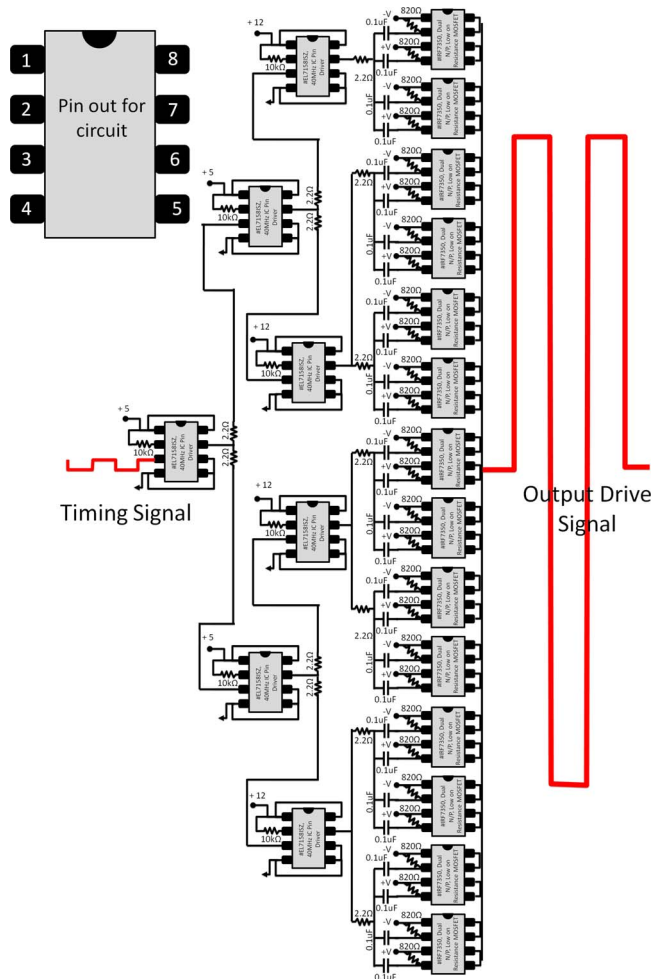


FIG. 1. (Color online) Schematic of the ultrasound driver. A TTL timed pin driver is used as a branching cascade to switch 14 low output impedance MOSFETs.

pling capacitors into the input pins 2 and 4 of the low on-resistance N-channel/P-channel MOSFET (IRF7350, International Rectifier Inc.). Pins 1 and 3 of the MOSFET are held at a maximum of -50 and $+50$ V, respectively, with 820 Ω resistors across pins 1–2 and 3–4. A 10 μF bypass capacitor to ground is applied as well to pins 1 and 3 of the MOSFET (not shown in Fig. 1). Pins 5–8 of the MOSFET are tied together and connected to the output drive signal through a standard BNC connector. The output impedance of ultrasound driver is determined from manufacturer's values of the MOSFETs. Measurements show it is almost entirely resistive and between 0.01 and 0.05 Ω . The input capacitance of the P-channel and N-Channel MOSFETs in parallel is 5.18 nF.

B. PCB design and construction

The PCB for the ultrasound driver is shown in Fig. 2, where components are outlined in white and their respective values are given in black. The PCB design is created using PCB123 LAYOUT V2 software from Sunstone Circuits Inc.

Pin drivers P1–P7 and MOSFETs M1–M14 are soldered to the board using an iron at 700 $^{\circ}\text{C}$. The remaining components, except for the 10 μF bypass capacitors in-line with the MOSFETs, are added in the same way. If electrolytic

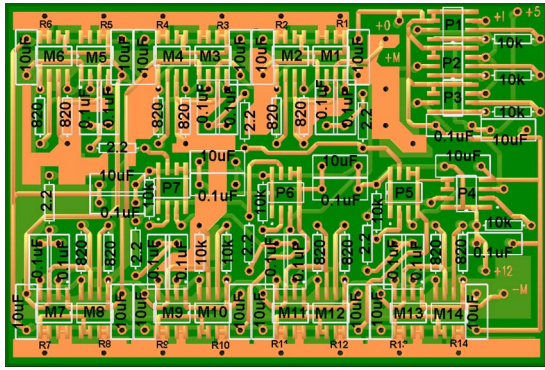


FIG. 2. (Color online) PCB layout for the ultralow-output impedance ultrasound driver (2×3 in.²). Components are shown in white with corresponding values in black text. Extra copper visible on the output of components M1–M14 is used for thermal dissipation and balancing.

capacitors are used, they must be installed with correct polarity. Heat sinks (3-050305U, Cool Innovations Inc.) with dimensions $4 \times 7 \times 5$ mm are attached to pairs of adjacent MOSFETs with thermally conductive Locktight epoxy (234476, Henkel) and activator (2301787387, Henkel). Thermal epoxy is applied to the bottom of the heat sinks, and activator is applied to the top surface of the MOSFETs. The heat sink and MOSFET are pressed together for 2 min. The in-line $10 \mu\text{F}$ bypass capacitors are then soldered in place. MOSFETs M1–M6 are in parallel on the PCB as are MOSFETs M7–M14. To make the entire array parallel, three 22 gauge copper wires are attached between vias R6 and R7, R5 and R8, and R4 and R9. The positive output from the driver at R14 and a ground point on the PCB are connected with a BNC connector.

Pin drivers P1–P3 are powered at +5 V, and P4–P7 are powered at +12 V. The input timing signal for the amplifier is supplied to the via marked +I in the top right of Fig. 2. The timing signal may be supplied by a crystal oscillator or function generator. The MOSFET switching supply is marked as holes +M and –M in Figure 2. The voltages supplied to +M and –M determine the output voltage range of the MOSFETs. The digital PCB file may be obtained from the authors on request.

C. Driver modeling

A Mason two T-port lossy transmission model adapted from Redwood¹⁹ and shown in Fig. 3 is used to characterize the electrical properties of the amplifier and piezoelectric transducers. The amplifier is a push-pull amplifier with output impedance R_{Source} . The acoustic energy emitted by the transducer is conducted through a water path. The frequency responses of the transducer and the water path are represented as two T-port models. Each model is composed of transcendental periodic functions of frequency that are chosen to be consistent with reflections of acoustic energy at intervals corresponding to the time required for signals to travel back and forth along the length of the acoustic path.

Starting from the output of the amplifier at R_{Source} , the model consists of a clamped capacitance of the piezoelectric material C_o .

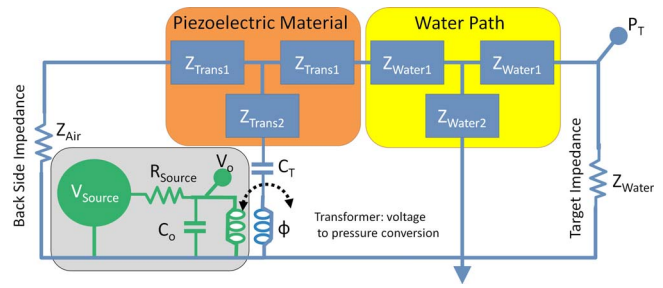


FIG. 3. (Color online) Mason model to study the effect of ultralow-output impedance amplifier driver in maximum power driving frequency. Amplifier output resistance R_{Source} is varied in this model from 0.03 to 200 Ω and the piezoelectric material is modeled as PZT-4 1.5 MHz and 8.0 MHz transducers. The piezoelectric material and water path are considered two port lossy transmission lines. The transformer converts electrical energy into pressure for the transducer conversion.

$$C_o = \frac{\epsilon_{33}^s \cdot A}{T_{pm}}, \quad (1)$$

where ϵ_{33}^s is the clamped dielectric constant for the material, T_{pm} is the thickness of the piezoelectric material (meters), and A is the radiating area of the piezoelectric element (square meters). C_o is placed in parallel to the transformer Φ in the model that converts the voltage into a mechanical

$$\text{pressure: } \phi = k_t \cdot v_{pm} \cdot C_o \cdot \sqrt{\frac{\rho_{pm}}{\epsilon_{33}^s}}, \quad (2)$$

where k_t is the thickness coupling coefficient for the material, v_{pm} is the velocity of sound in the piezoelectric material (m/sec^2), and ρ_{pm} is the density of the piezoelectric material (kg/m^3).

The transformer Φ in series with negative capacitance C_T , represents the pressure output of the piezoelectric transducer, as in Redwood¹⁹ where $C_T = -C_o / \phi^2$.

The piezoelectric material T-port model shown in Figure 3 is modeled as

$$Z_{\text{Trans } 1} = Z_{pm} \cdot \tanh \left[\frac{\Gamma_{pm}(\omega) \cdot T_{pm}}{2} \right], \quad (3)$$

$$Z_{\text{Trans } 2} = Z_{pm} \cdot \csc h[\Gamma_{pm}(\omega) \cdot T_{pm}], \quad (4)$$

$$Z_{pm} = A \cdot \rho_{pm} \cdot v_{pm}, \quad (5)$$

$$\Gamma_{pm} = \alpha_{pm} + j\beta_{pm}, \quad (6)$$

$$\alpha_{pm} = \frac{\beta_{pm}}{2Q_m}, \quad (7)$$

and

$$\beta_{pm} = \frac{\omega}{v_{pm}}, \quad (8)$$

where Z_{pm} is the characteristic acoustic impedance of the piezoelectric material, Γ_{pm} is the material propagation vector, α_{pm} and β_{pm} are the attenuation coefficients in the material, ω is the radian frequency variable, and Q_m is the mechanical quality factor for the piezoelectric material. Values for the constants used in the model are provided in Table I.

The water path T-port model in Fig. 3 is modeled as

TABLE I. Compiled constant values and units used in the model presented.

	Symbol	Value	Units
Amplifier properties			
Voltage supply	V_{Source}	10	v
Output impedance	R_{Source}	Variable	Ω
Radian frequency variable	ω	Variable	rads
Piezoelectric properties			
Clamped dielectric	ϵ_{33}^S	7.17×10^{-10}	N/A
Thickness of piezoelectric	T_{pm}	Variable	m
Radiating area	A	Variable	m ²
Thickness coupling coefficient	k_r	0.42	N/A
Velocity of sound in the piezoelectric material	v_{pm}	4420	m/s
Density of the piezoelectric material	ρ_{pm}	7500	kg/m ³
Mechanical quality factor for material	Q_m	128	N/A
Water path properties			
Velocity of sound in water	v_w	1540	m/s
Density of water	ρ_w	1000	kg/m ³

$$Z_{\text{Water } 1} = Z_{wm} \cdot \tan h \left[\frac{\Gamma_{wm}(\omega) \cdot T_{wm}}{2} \right] \quad (9)$$

and

$$Z_{\text{Water } 2} = Z_{wm} \cdot \csc h[\Gamma_{wm}(\omega) \cdot T_{wm}]. \quad (10)$$

The terms for the water path model impedances $Z_{\text{Water } 1}$ and $Z_{\text{Water } 2}$ are similar to the transducer material [Eqs. (3)–(8)] with similar meanings, however, with different constant values as provided in Table I.

The transducer is air-backed and is included in the model as a small backside impedance Z_{Air} so that mechanical energy is reflected in the forward direction toward the water target with its characteristic impedance Z_{Water} . The value of Z_{Air} is chosen to match the models prediction of the actual electrical impedance properties of the ultrasound transducer used in this study. For the model $Z_{\text{Air}} = 0.38 \times Z_{\text{Water}}$, where $Z_{\text{Water}} = A \cdot \rho_w \cdot v_w$.

From the circuit in Fig. 3, two node voltages may be defined. By using conventional circuit theory and summing the currents at the two node points, two equations and two unknowns result. These can be related to the input drive voltage in matrix notation. The matrix equation can then be solved for the two unknown quantities, and the input and output power may be determined from an examination of the circuit model. Thus one can write for the output and input powers

$$\text{PowerOut} = \frac{P_T(\omega)^2}{R_{\text{Water}}}, \quad (11)$$

where P_T is the voltage (or pressure) across R_{Water} and

$$\text{PowerIn} = I_S(\omega) \cdot V_o(\omega) \cdot \cos(\theta), \quad (12)$$

where $I_S = [V_S - V_o(\omega)]/R_S$ and $\theta = \text{angle}(V_o) - \text{angle}(I_S)$. The efficiency of the amplifier is calculated by

$$\text{Efficiency} = \frac{\text{PowerOut}(\omega)}{\text{PowerIn}(\omega)}. \quad (13)$$

The Mason model often is used in ultrasonics to help develop transducer front and back matching layers, tune electrical networks, and estimate transducer transmit and receive impedances. Here, we use the model to predict the maximum power output and efficiency of the ultralow-output impedance driver and to compare it with 50 Ω and impedance-matched amplifier sources when driving transducers. We varied the amplifier source impedance R_{Source} from 0.03 to 100 Ω and predicted the output power of four different PZT-4 transducers into a water target impedance R_{Water} . The characteristic frequency of the transducer was varied from 1.5 to 8.0 MHz, which simulates variations in the thickness of the piezoelectric transducers. The resonant electrical impedance of the transducer was varied between 0.37 and 10.6 Ω , which simulates variations in the transducer's cross-sectional area. The drive source V_S is taken as 10 V. Parameters for the model transient function constants including $Z_{\text{Trans } 1}$, $Z_{\text{Trans } 2}$, $Z_{\text{Water } 1}$, and $Z_{\text{Water } 2}$ are compiled in Table I, and were obtained from Redwood¹⁹ and EBL Products Inc. for an air-backed PZT-4 transducer into a water bath target.

D. Measurements of low output impedance ultrasound driver

The amplifier is tested by connecting the input (+I hole) to a function generator (Tektronix #ARG3102) and powering it with multiple adjustable power supplies (Agilent 6613C) for the +5, +12, and \pm MOSFETs power. MOSFET switching power is varied from 10 to 50 V_{pp} . Current drawn from the circuit is measured using the power supply current meter. The amplifier is tested in pulse and continuous wave mode by varying the TTL timing signal input. The output waveform and power spectrum of the driver are collected using an oscilloscope (Tektronics TDS2002B) with a 1.54 MHz lead zirconate titanate (PZT-4) piezoelectric ceramic (EBL Products Inc.). The ceramic is 0.75 in. in diameter with a 1.5 in. radius of curvature and the 12 Ω electrical impedance is measured by impulse impedance spectroscopy. The ultrasound probe is attached to the output and placed in an acoustically insulated water bath.¹ The drive waveform is also measured with 12 and 50 Ω power resistors in series with the transducer probe to compare impedance matching techniques with the ultralow-output impedance driver. The output impedance, resistance, and reactance of the amplifier are measured by attaching a 12 Ω power resistor across the output of the amplifier and measuring the phase and voltage changes across the component at drive frequencies from 0 to 8 MHz. The ultrasonic power output from the 1.54 MHz transducer is determined in continuous wave operation by measuring the force that the ultrasound exerts on an acoustic absorbing object.²¹ We compare results to electrical measurements of power, using measured electrical impedance properties of the 1.54 MHz probe²² and the ultrasonic power conversion efficiency from the Mason model.^{1,19,20}

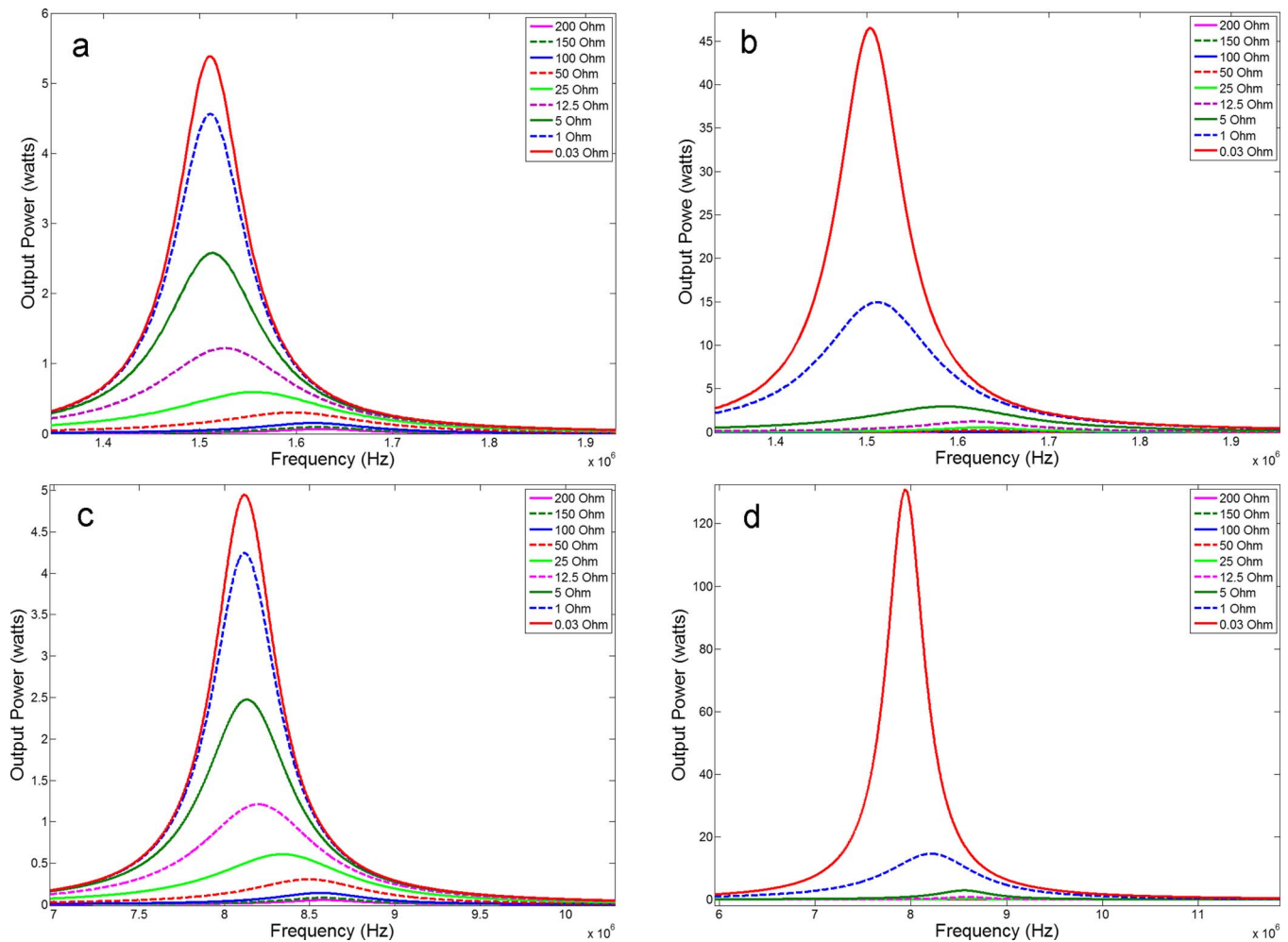


FIG. 4. (Color online) Predictions of the model shown in Fig 3. (a)–(d) show the maximum output power as a function of frequency for values of the amplifier source impedance R_{Source} in the range 0.03–200 Ω . (a) 1.5 MHz 10.3 Ω transducer. (b) 1.5 MHz 1.2 Ω transducer. (c) 8 MHz 10.6 Ω transducer. (d) 8 MHz 0.37 Ω transducer.

III. RESULTS

A. Model results

The predictions of the Mason model are shown in Fig. 4. Figures 4(a)–4(d) show the computed maximum output power from the transducer as a function of frequency for two transducers. Figures 4(a) and 4(b) pertain to a 1.5 MHz transducer with 10.3 and 1.2 Ω resonant electrical impedance, respectively. Figures 4(c) and 4(d) pertain to an 8.0 MHz transducer with 10.6 and 0.37 Ω resonant electrical impedance, respectively.

In every case the maximum power delivered to the transducer and, hence, the maximum acoustic energy generated by the device, are obtained for the smallest value of R_{Source} . The maximum acoustic power is determined by the piezoelectric transducer efficiency, which was estimated as 63% from input to output power ratios in the model. The electrical impedance of the piezoelectric also affects the maximum acoustic power according to

$$\text{PowerOut} \approx \frac{V_o^2}{Z}, \quad (14)$$

where PowerOut is the acoustic power from the transducer, V_o is the voltage across the transducer, and Z is the electrical

impedance of the transducer. In this case, increasing the cross-sectional area of the transducer decreases the electrical impedance Z and increases acoustic power. Figure 4 shows that for small R_{Source} , the maximum acoustic power is obtained at the transducer's natural axial resonance frequency. For larger values of R_{Source} , maximum power occurs at frequencies slightly higher than the resonance frequency, especially for the 8.0 MHz transducer.

B. Ultrasound driver performance

The output waveform of the ultralow-output impedance ultrasound driver at the 20 V_{pp} power setting is shown for 1.54 and 8 MHz TTL timing signals in Figs. 5(a) and 5(d), respectively. Figure 5(b) is the measured output waveform from the driver while connected to a PZT-4, 1.54 MHz, and 0.75 in. diameter piezoelectric ceramic used in this and prior studies.^{1,7,8} Figure 5(c) is the power spectrum measurement from the waveform of Fig. 5(b). The waveform of the 1.54 MHz drive signal [Figs. 5(a) and 5(b)] shows slight ringing at the corners without and with the ultrasound transducer attached to the output. Overall, the 1.54 MHz driving signal is reasonably clean with no oscillations in the waveform and fast rise times between the push-pull cycles. No measurable

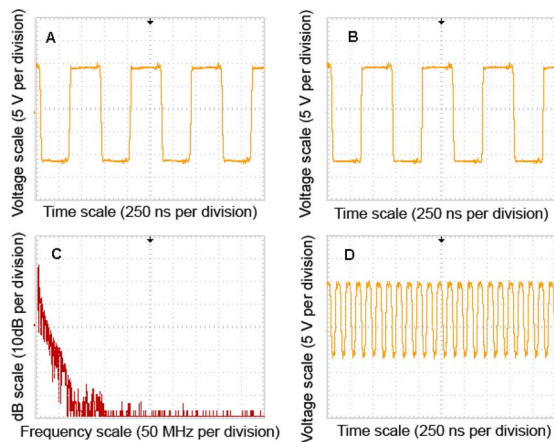


FIG. 5. (Color online) (a) and (b) Measured 1.54 MHz output waveform from the ultrasound driver with slight ringing at the corners without and with the ultrasound transducer attached, respectively. (c) The power spectrum of the 1.54 MHz waveform. The drive signals energy concentration is in the early megahertz frequencies. (d) Measured 8.0 MHz signal shows attenuated drive voltage and asymmetry of the waveform with oscillations on both the positive and negative sides.

voltage drop or phase shift is noticeable between Figs. 5(a) and 5(b), showing the amplifier design has a very low output resistance and reactance. The power spectrum in Fig. 5(c) is representative of a square-wave drive signal with slight corner signal spiking. Figure 5(d) shows that the amplitude of the driver is attenuated by approximately 20% for the higher frequency of 8 MHz. Furthermore, the waveform is asymmetric and exhibits small oscillations for positive and negative sides. When the TTL timing frequency is increased into the 10 MHz range, the MOSFETs saturate and are unable to switch at these speeds. The output resistance and reactance of the device was measured to be less than 0.05Ω and almost entirely real with no measurable phase shift.

Figure 6 compares the performance of the driver when adjusting the output impedance of the driver to match the transducer. Clearly, this is reverse impedance matching, since generally one matches the transducers impedance to the amplifiers output impedance. Figures 6(a) and 6(b) show the amplifier output without reverse impedance matching. Figure 6(a) gives the output without a transducer attached and Figure 6(b) gives the output with the 1.54 MHz ultrasound transducer attached to the driver at $17 V_{pp}$ power setting. The output of the amplifier is effectively transmitted with a clean signal and 99% voltage transfer. Figures 6(c) and 6(d) show output waveforms from the driver when a 12Ω power resistor is attached to the driver in series with the 12Ω ultrasound transducer without and with the transducer attached, respectively. Signal distortion is present in Fig. 6(d) with 62% voltage transfer from driver. Figures 6(e) and 6(f) show output waveforms from the driver when a 50Ω power resistor is attached to the driver in series with the 12Ω ultrasound transducer without and with the transducer attached, respectively. Signal distortion in Fig. 6(f) is similar to that observed in Fig. 6(d) for the 12Ω resistor, but in this case, voltage transfer to the transducer is reduced to 22%. These results show the ultralow-output impedance driver performs best without matching the drivers' output impedance to the transducer. However, it could be advantageous to

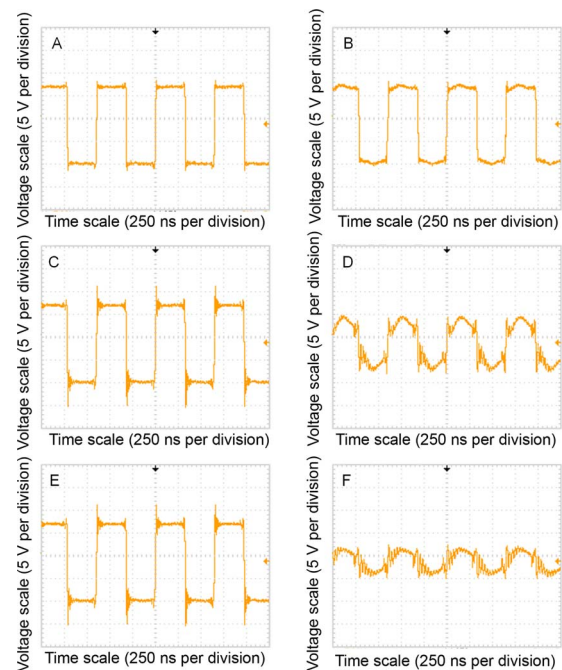


FIG. 6. (Color online) (a) and (b) Measured 1.54 MHz output waveform from the ultrasound driver with slight ringing at the corners without and with the ultrasound transducer attached, respectively. (c) and (d) Output waveform from the ultrasound driver with 12Ω impedance matching power resistor attached directly to driver in series to the 12Ω ultrasound transducer without and with the transducer attached, respectively. (e) and (f) Output waveform measured with 50Ω power resistor in series without and with transducer, respectively.

match the transducers input impedance to the ultralow-output impedance of the driver by minimizing Z as predicted in Eq. (14), thereby maximizing the output power from the driver. Minimizing Z would also result in energy waste across the amplifiers output impedance because of voltage division, and may not be appropriate for portable battery powered applications.

The temporal-average acoustic output power from the 1.54 MHz ultrasound probe while driven at $50 V_{pp}$ is 48.0 W, as determined from a force balance. Using electrical measurements of power and the electroacoustic efficiency of 63% from the Mason model gives an output power of 33.0 W. The driver has a turn on delay of 10 ms due to capacitor coupling between pin driver and MOSFETs. Once on, it is capable of providing short bursts of acoustic energy for less than 5 ms and for continuous wave operation. The finished driver operating at $28 V_{pp}$ with the transducer used in this study is shown in Figs. 7(a) and 7(b). Figure 7(a) shows the driver powering the 1.54 MHz transducer with a clean waveform and visually noticeable acoustic energy causing the water to vaporize. Figure 7(b) is a close-up of the transducer in the water bath levitating and cavitating the water molecules into the air.

IV. DISCUSSION

A. Amplifier design

Managing the heat generated in the ultralow-output impedance amplifier is essential for its sustained operation. The outputs of the 14 parallel MOSFETs are electrically and

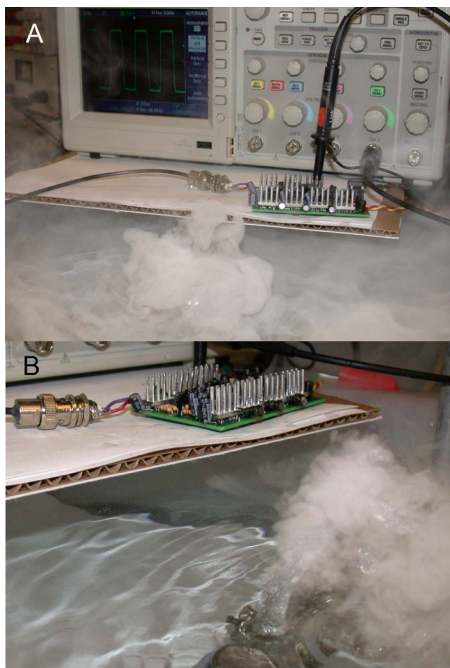


FIG. 7. (Color online) Complete high-power ultralow-output impedance ultrasound driver powering a 1.54 MHz ultrasound transducer. (a) Ultrasound driver operating at 28 V_{pp} with a clean waveform and high acoustic energy output causing the water to vaporize. (b) Close-up of the transducer in the water bath levitating and cavitating the water molecules into the air. Cavitation bubbles are visible in the water stream off the front face of the transducer.

thermally connected with heat-sinking plains built directly into the PCB. The heat-sinking plains dissipate heat generated from switching losses in the MOSFETs and balance the temperature distribution between individual MOSFETs to prevent thermal runaway and damage to the integrated circuits. Thermal management external heat sinks that are attached to the top surface of the MOSFETs in groups of two are not necessary for low power applications in the range 0–10 W or for low driver frequency in the range 0–3 MHz. However, for high-power applications in the range 20–60 W and for high driver frequency in the range 4–8 MHz, externally applied heat sinks are necessary for continuous wave operation as shown in Fig. 7.

B. Modeling results of acoustic output power

The Mason model predicts that decreasing the output impedance of the driver source causes a shift in the drive frequency for maximum acoustic output power, as shown in Fig. 4. The shift can be measured experimentally by using a 50 Ω output impedance function generator to drive the PZT-4, 1.54 MHz probe used in this study and comparing results with the ultralow-impedance amplifier. The shift in maximum drive signal power from the actual electrical resonance of the transducer is approximately 85 kHz for the 50 Ω driver. Although the magnitude of this shift seems modest, the results in Fig. 4 suggest small shifts in the maximum power driver frequency can have significant effects on the output power achieved. For example, if a system is constructed to produce 1.5 MHz ultrasound with a 1.5 MHz piezocrystal and standard 50 Ω driving electronics to

complement the frequency, over 50% of the input energy may be lost, as seen in Fig. 4(a) by comparing the peak value of the 50 Ω curve (approximately 0.5 W) to the power at 1.5 MHz (approximately 0.25 W). With impedance matching circuitry corresponding to the 12.5 Ω curve in Fig. 4(a), the power loss in driving at the incorrect frequency is about 20%. With ultralow-impedance drivers the maximum power drive is closely matched to the electrical resonance of the transducer as shown in Figs. 4(a)–4(d), and this problem is mitigated

C. Ultralow-impedance ultrasound driver

The ultrasound driver is useful in myriad applications that require both low and high-power acoustic applications. Each amplifier can be constructed for under \$100.00. Since the ultralow-impedance driver delivers 99% of the voltage from the power supply to the transducer, batteries may be used to power the system in high and low power applications. The International Rectifier's low on-resistance MOSFET # IRF7350 can withstand 100 V_{pp} operation, according to the manufacturer, which could provide more than 10 A of current. At 100 V_{pp}, our acoustic efficiency model estimates that the amplifier could produce an acoustic power of 130 W from the transducer used in this study.

The circuit drives existing transducers more efficiently than typical push-pull type amplifiers using impedance matching circuitry and rf amplifiers. If possible, however, it is beneficial to use ultralow-impedance coax-cabling to connect the transducer to the ultralow-impedance amplifier to maximize energy transfer and minimize waste in the form of heat. This will be important in implementing the ultralow-impedance amplifier into efficient and portable therapeutic ultrasound applications.^{1,17,23}

V. CONCLUSIONS

Modeling and experiments show that the ultralow-impedance amplifier delivers maximum power close to the electrical resonance of the ultrasound transducer. This is important in designing systems that are efficient at producing ultrasonic energy to limit energy waste and maximize energy transfer at low voltages.

The ultralow-impedance ultrasound driver and PCB is considerably smaller (2 × 3 in.²) than typical rf amplifiers, is significantly less expensive, requires only dc power supplies, and is 99% efficient at delivering the source voltage across the ultrasound transducer. The amplifier can operate in the range from 0 to 8 MHz, which spans the relevant range for medical therapeutic ultrasound and HIFU systems. The ultralow-impedance driver has an output impedance of 0.01–0.05 Ω and provides switching of up to 100 V_{pp}. The amplifier can provide 48 W of acoustic energy from the 1.54 MHz transducer using no impedance tuning and has the potential to provide over 130 W of power using larger piezocrystals and higher voltage power supplies.

ACKNOWLEDGEMENTS

The authors would like to thank Cool Innovations Inc., Henkel Inc., and EBL Products Inc. for supplying heat sinks,

thermally conductive epoxy, and piezoelectric material, respectively. This research was supported in part by the National Science Foundation Graduate Fellowship Program and the Cornell University Presidential Life Science Fellowship.

APPENDIX: Parts list for amplifier components

1. PCB, quantity 1 (Sunstone Circuits Inc.)
2. Low output impedance MOSFET, quantity 14 (#FDS4559, Fairchild Semiconductor Inc. of #IRF7350, International Rectifier Inc.)
3. Pin driver, quantity 7 (#EL7158ISZ, Intersil Inc.)
4. 10 k Ω , $\pm 5\%$, 1/4 watt resistor, quantity 7 (General)
5. 820 Ω , $\pm 5\%$, 1/4 watt resistor, quantity 14 (General)
6. 2.2 Ω , $\pm 5\%$, 1/4 watt resistor, quantity 8 (General)
7. 10 μF , $\pm 20\%$, 50 volt electrolytic capacitor, quantity 19 (General)
8. 0.1 μF , $\pm 20\%$, 50 volt electrolytic capacitor, quantity 19 (General)
9. BNC connector, quantity 2 (General)
10. Heat sinks, quantity 7 (#3-050305U Cool Innovations Inc.)
11. Thermal conductive epoxy, quantity 25 ml (Locktight idh#234476 3873, Henkel Inc.)
12. Activator, quantity 13 ml (Locktight, idh#230178 7387, Henkel Inc.)

¹G. K. Lewis and W. L. Olbricht, *Rev. Sci. Instrum.* **79**, 114302 (2008).

²J. Wu and W. L. M. Nyborg, *Ultrasonics in Medicine* (World Scientific, Singapore, 2006).

³G. Aus, *Eur. Urol.* **50**, 927 (2006).

⁴S. Mitragotri, *Nat. Rev. Drug Discovery* **4**, 255 (2005).

⁵M. R. Bailey, V. A. Khokhlova, O. A. Sapozhnikov, S. G. Kargl, and L. A. Crum, *Acoust. Phys.* **49**, 369 (2003).

⁶E. J. Park, K. I. Jung, and S. W. Yoon, *J. Acoust. Soc. Am.* **107**, 2788 (2000).

⁷G. K. Lewis, Jr., W. Olbricht, and G. K. Lewis, *J. Acoust. Soc. Am.* **2**, 1 (2008).

⁸G. K. Lewis, Jr., P. Wang, G. K. Lewis, and W. Olbricht, *Proceedings of the International Symposium on Therapeutic Ultrasound* (AIP, New York, 2008).

⁹C. M. H. Newman and T. Bettinger, *Gene Ther.* **14**, 465 (2007).

¹⁰G. ter Haar and C. Coussios, *Int. J. Hyperthermia* **23**, 89 (2007).

¹¹N. I. Vykhodtseva, K. Hynynen, and C. Damianou, *Ultrasound Med. Biol.* **21**, 969 (1995).

¹²D. Cesario *et al.*, *Atrial Fibrillation*, Contemporary Cardiology (Humana, Totowa, New Jersey, 2008), Chap. 15, pp. 199–207.

¹³H. R. Guzman, D. X. Nguyen, A. J. McNamara, and M. R. Prausnitz, *J. Pharm. Sci.* **91**, 1693 (2002).

¹⁴K. Keyhani, H. R. Guzman, A. Parsons, T. N. Lewis, and M. R. Prausnitz, *Pharm. Res.* **18**, 1514 (2001).

¹⁵J. Sundaram, B. R. Mellein, and S. Mitragotri, *Biophys. J.* **84**, 3087 (2003).

¹⁶S. Vaezy, X. Shi, R. W. Martin, E. Chi, P. I. Nelson, M. R. Bailey, and L. A. Crum, *Ultrasound Med. Biol.* **27**, 33 (2001).

¹⁷N. R. Owen, M. R. Bailey, B. J. P. Mortimer, H. Kolve, J. Hossack, and L. A. Crum, in *Proceedings of the Third International Symposium on Therapeutic Ultrasound*, 2003 (unpublished), pp. 399–404.

¹⁸“Why 50 Ω ?,” Microwave Encyclopedia, www.microwaves101.com (2008).

¹⁹M. Redwood and J. Lamb, *Proc. IEEE* **103**, 773 (1956).

²⁰S. A. Morris and C. G. Hutchens, *IEEE Trans. Ultrason. Ferroelectr. Freq. Control* **33**, 295 (1986).

²¹S. Maruvada, G. R. Harris, and B. A. Herman, *J. Acoust. Soc. Am.* **121**, 1434 (2007).

²²G. K. Lewis, Jr., G. K. Lewis, Sr., and W. Olbricht, *Meas. Sci. Technol.* **19**, 105102, (2008).

²³G. K. Lewis, Jr. and W. Olbricht, *J. Acoust. Soc. Am.* **5**, 1, (2008).